Wind Turbine Generator Emulator with Current Control mode

Satoshi Nagai, Kouki Tokui, Hiroki Watanabe, Jun-ichi Itoh
Dept. of Electrical, Electronics and Information Engineering
Nagaoka University of Technology
Niigata, Japan
satoshi_nagai@stn.nagaokaut.ac.jp, k_tokui@stn.nagaokaut.ac.jp, hwatanabe@vos.nagaokaut.ac.jp, itoh@vos.nagaokaut.ac.jp

***Abstract*—This paper proposes an emulator for a wind turbine generator with a current control mode to emulate a current source. In this paper, the emulator uses the current control mode without voltage controller to consider the generator as a current source. The emulator is used to verify the power converter connected to the wind turbine. A three-phase inverter with the current controller is applied in the emulator of the wind turbine generator. In addition, the current control command of the emulator is calculated from the motor equation using the emulator output voltage detection value. Furthermore, the output filter of the emulator is only used inductor. Therefore, low-pass filter composed by RC filter with low cutoff frequency compared with the switching frequency is applied to the emulator voltage detection. In the experimental results, the emulator operates in accordance with the motor equation when the current control response of the emulator and test converter are 4000 rad/s and 100 rad/s. The error voltage between the measurement and theoretical value is less than 17.5% in the experimental results.**

Keywords—Wind turbine emulator; Current control; Motor equation;

I. INTRODUCTION

In recent years, distributed generation systems such as the wind turbine systems have been actively researched for energy saving with renewable energy [1-7]. The wind turbine systems supply the power to the load with the grid-tied converters [8-11] connecting the power grid. However, the wind turbine with blades are not applied to verify the test converter in the view point of the scale for the equipment. In addition, the wind turbine system applies a generator such as a permanent magnetic synchronous machine (PMSM) [12-13]. Therefore, the verification of the grid-tied converter is not easy to achieve, because the preparation of the generator is also necessary. On the other hand, there is a case to apply an emulator which operates as the wind turbine system. The emulator which is composed by converters is applied to simulate the power source or load, when the actual power source or load should not be used [14-18]. The emulator plays the actual behavior of the power source.

In [15], a control method is proposed for a synchronous generator emulator. The ideal transformer method [19] and the feedback current filtering method [20] are applied in the proposed control method. The experimental results of the generator emulator phase voltage, current, angular velocity, and torque are match to the simulation results in steady state and transient operation. However, the control delay may occur due to the feedback current filtering method when the virtual generator operation is compared with the actual generator. In [16], a control method is proposed for a load emulator of the power grid. In this paper, the load emulator operates as a constant-impedance, constant-current, constant-power model, and a three-phase induction motor model. Moreover, the emulator operates with the current command derived by the emulation model equation [21-22]. However, the detail of the current command calculation for the emulator has not been shown in this paper.

This paper proposes the emulator of the wind turbine with the current control mode without a voltage control. In this paper, the emulator operation is verified to the wind turbine system composed by PMSM. The original idea of the proposed system is that the emulator uses only the current control mode in order to operate as the current source. The current command is derived by the motor equation with the output voltage of the emulator. In addition, the interference of the current control response between the emulator and the connected converter has to be considered. The emulator operation is demonstrated by separating the current control response between the emulator and the connected converter in the experiments. As the results, the emulator is demonstrated with the operation based on the motor equation when the current control responses of the emulator and connected converter are 4000 rad/s and 100 rad/s.

II. SYSTEM COMPONENTS OF WIND TURBINE EMULATOR

Figure 1 shows the circuit configuration of the emulator for the wind turbine system. Note that V_{in} is the input voltage of the emulator, $i_{u\mathrm{det}}$, $i_{v\mathrm{det}}$, and $i_{w\mathrm{det}}$ are the output phase current, $v_{u\mathrm{det}}$, $v_{v\mathrm{det}}$, $v_{w\mathrm{det}}$ are the output voltage of the emulator, L is the output filter inductance, respectively. The emulator is composed by the isolated DC/DC converter and the three-phase voltage source inverter (3Φ VSI). In this paper, a dual active bridge converter is applied as the isolated DC/DC converter. The voltage control is applied in the inverter side of the DC/DC converter to control the DC-link voltage for 3Φ VSI in constant value. Moreover, a three-phase three-level neutral-point-clamped (NPC) inverter is applied as 3Φ VSI. The three-phase three-level NPC inverter is applied to reduce the current

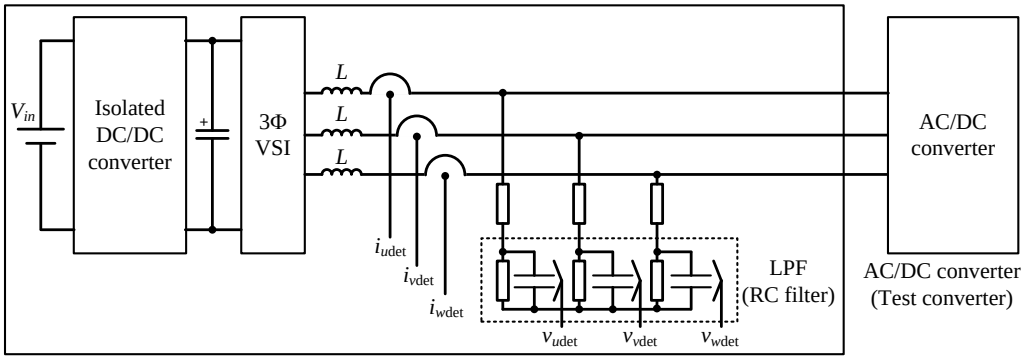

Fig. 1. Constitution of emulator for wind turbine system. The emulator is composed by an isolated DC/DC converter and a 3Φ VSI. In addition, the test converter is composed by a AC/DC converter.

ripple for switching frequency component and increase the output voltage in the future. This paper focuses on the current control of 3Φ VSI. In addition, a three-phase AC to DC converter (test converter) is applied as the grid-tied system. The three-phase two-level converter is applied as the test converter. Moreover, the wind turbine system has to detect the fundamental components of the output voltage. However, the output voltage is pulse width modulation (PWM) waveform without the output filter such as the LC filter or LCL filter. Furthermore, the control model becomes change when the LC or LCL filter is applied in the output filter. Thus, the RC filter as the low-pass filter (LPF) is applied in the three-phase voltage detection. The cutoff frequency of the RC filter is set to the low frequency in order to detect the fundamental component of the output voltage without the switching frequency components.

Figure 2 shows the control block diagram of the current controller for the emulator. Note that L is the inductance of 3Φ VSI, s is the Laplace operator, $v_{d\mathrm{det}}$ and $v_{q\mathrm{det}}$ are the voltage detection value of dq axis, $i_{d\mathrm{ref}}$ and $i_{q\mathrm{ref}}$ are the current commands calculated from the motor equation, $i_{Ld\mathrm{det}}$ and $i_{Lq\mathrm{det}}$ are the detection value for the 3Φ VSI output current, $v_{d\mathrm{det}}$ and $v_{q\mathrm{det}}$ are the detection value for the output voltage, v_d and v_q are the output voltage, i_{Ld} and i_{Lq} are the output current, PI is the PI controller, ω is the rotation speed of the motor, θ is the phase information, θ_{LPF} is the phase delay due to the LPF, and θ' is phase information for dq transform of the output voltage, respectively. The PI controller composed by following equation

$$\begin{aligned} \mathrm{PI} &= K_p + \frac{K_p}{sT_i} \\ K_p &= 2\zeta\omega_{em}L \\ T_i &= \frac{2\zeta}{\omega_{em}} \end{aligned} \quad (1),$$

where K_p is the proportional gain, T_i is the integral time, s is Laplace operator, ζ is the damping coefficient, ω_{em} is the current control angular frequency, respectively. Moreover, the motor equation is expressed as follows.

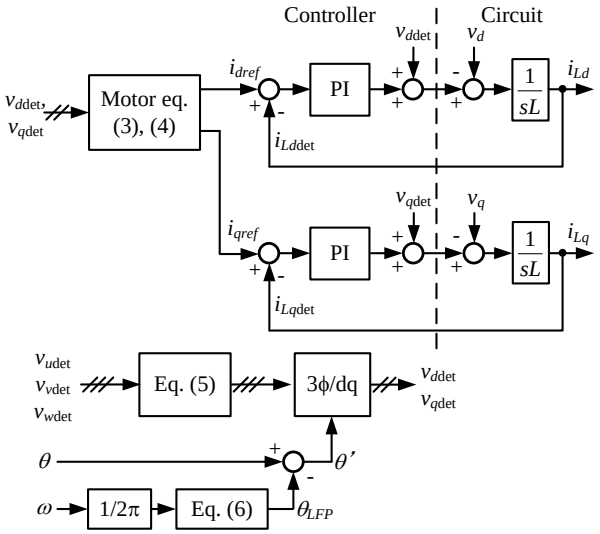

Fig. 2. Control block diagram of current controller for emulator. The current commands are derived by the motor equation with the output voltage.

$$\begin{bmatrix} vd \\ vq \end{bmatrix} = \begin{bmatrix} R & -\omega L_q \\ \omega L_d & R \end{bmatrix} \begin{bmatrix} i_d \\ i_q \end{bmatrix} + \begin{bmatrix} 0 \\ \omega\phi \end{bmatrix} \quad (2)$$

The power flow of the generator is reversed compared with the motor. Thus, the generator equation is derived by reversing the power flow in (2). Therefore, the wind turbine generator applies the motor equation in (2). The current commands of the emulator are expressed from (2) as follows

$$i_{dref} = \frac{Rv_{d\,\mathrm{det}} + \omega L_q v_{q\,\mathrm{det}} - \omega^2 L_q \phi}{R^2 + \omega^2 L_d L_q} \quad (3)$$

$$i_{qref} = \frac{Rv_{q\,\mathrm{det}} - \omega L_d v_{d\,\mathrm{det}} - R\omega\phi}{R^2 + \omega^2 L_d L_q} \quad (4),$$

where R is the resistance of the motor, ϕ is back emf coefficient, and L_d and L_q are the inductance of d and q axis, respectively. In the case, the transient terms are ignored in the motor equation. Moreover, LPF with the low-cutoff frequency compared with the switching frequency is attached in the output voltage detection circuit. Thus, it is necessary to consider the compensation of both the gain and phase delay for the output frequency. The compensation equations of the LPF gain G_{LPF} and phase delay θ_{LPF} are expressed as

$$G_{LPF} = \sqrt{\left(f_{out} / f_{LPFcut} \right)^2 + 1} \tag{5}$$

$$\theta_{LPF} = \tan^{-1}\left(f_{out} / f_{LPFcut} \right) \tag{6},$$

where f_{out} is the output frequency of the emulator, f_{LPFcut} is the cutoff frequency of LPF. (5) is multiplied in the voltage detection value, and (6) is subtracted from the phase information to transform the dq axis.

Figure 3 shows the control block diagram of the test converter. The test converter is composed by the current controller applying the PI controller. Note that i_{dout}^* and i_{qout}^* are the input current commands of the d and q axis, i_{dout} and i_{qout} are the input current of the d and q axis, i_{dout_det} and i_{qout_det} are the input current detection values of the d and q axis, PI_d and PI_q are the PI controller of the d and q axis, respectively. The PI controllers in the test converter are composed as follows equations

$$\begin{aligned} \mathrm{PI}_x &= K_{px} + \frac{K_{px}}{sT_{iconv}} \\ K_{px} &= 2\zeta\omega_{conv}L_x - R \qquad (x:\ d,\ q) \\ T_{iconv} &= \frac{2\zeta}{\omega_{conv}} \end{aligned} \tag{7},$$

where K_{px} is the proportional gain of d or q axis, T_{iconv} is the integral time, ω_{conv} is the angular frequency of the current controller for the test converter, respectively. The current controller does not use the disturbance compensation. Moreover, the current control model is composed by the inductance and winding resistance. In addition, the synchronous of the phase between the emulator and test converter is achieved by detecting the phase information from the generator emulator.

III. Simulation of Wind Turbine Generator Emulator

From simulation of the emulator, the wind turbine generator emulator is verified to the operation based on the current command generated by equation (3) and (4).

Table I shows the simulation conditions of the emulator. Note that two LPF are applied in the voltage detection circuit to greatly reject the high frequency components such as the switching frequency components in the simulation. The cutoff frequencies for the two LPF are 800 Hz and 1300 Hz, respectively.

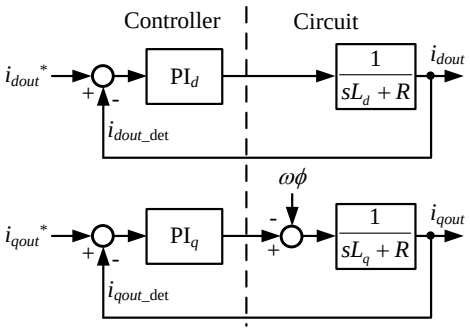

Fig. 3. Control block diagram of current controller for test converter. The current controller does not apply the disturbance compensation such as feedfoward. Moreover, the current controller is operated in the low control response.

TABLE I. Simulation and Experimental Conditions.

Motor parameter		
Resistanse	R	5.7 Ω
Inductance	L_d	43.5 mH
	L_q	114 mH
Buck emf coefficient	ϕ	0.54 Vs/rad
Output frequency	f_{out}	10 Hz
Emulator		
Carrier frequency	f_{c_em}	6 kHz
Current control response	ω_{em}	4000 rad/s
Output inductance	L_f	10 mH
Cutoff frequency of LPF for voltage detection	f_{LFPcut_1}	800 Hz
	f_{LFPcut_2}	1300 Hz
Test converter		
Carrier frequency	f_{c_conv}	10 kHz
Current control response	ω_{conv}	100 rad/s

Figures 4 and 5 show the simulation results of the emulator operation. Note that the emulator output voltage in Fig. 4(a) and Fig. 5(a) are the waveforms which the harmonics such as the switching frequency components were rejected by LPF. From each simulation result, the emulator output current follows each current command value (Fig. 4: $i_{dout}^* = 2$ A, $i_{qout}^* = 0$ A, Fig. 5: $i_{dout}^* = 0$ A, $i_{qout}^* = -2$ A). Thus, the emulator current command is generated by following the test converter current command. Then, the emulator current is controlled by the generated current command. However, the emulator current command has error for the test converter current command. The error is caused by such as the delay time for the discretization and the non-implementation of the disturbance compensation.

Table II shows the comparison of the emulator output voltage between the simulation values and theoretical value based on the motor equation. The theoretical values in Table

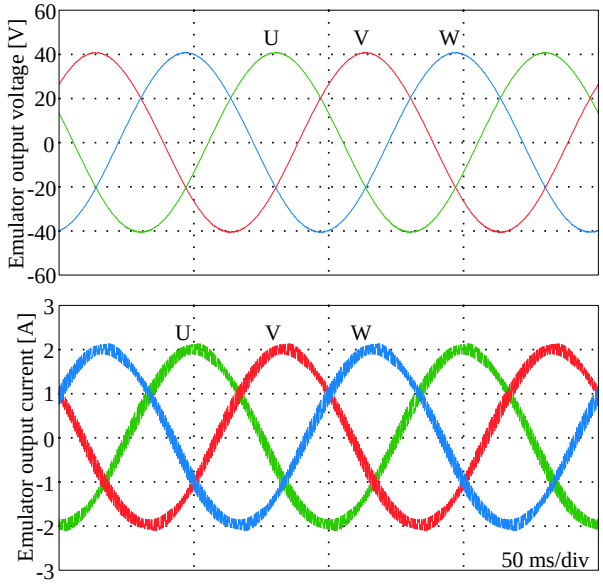

(a) Emulator output voltage and current.

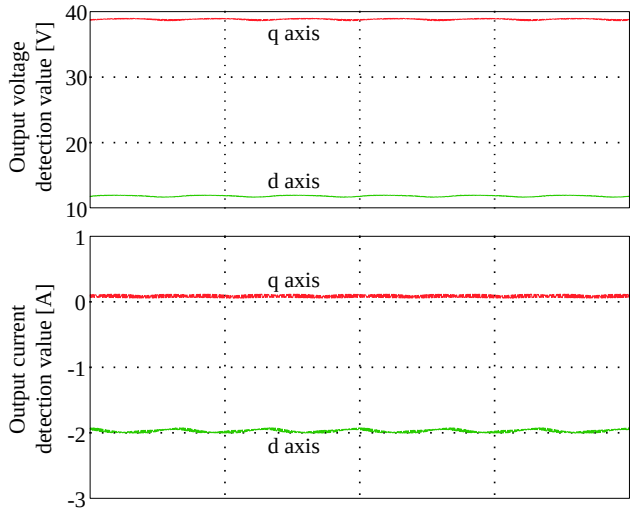

(b) Emulator output voltage and current detection value (dq axis).

Fig. 4. Simulation waveforms for wind turbine emulation. The current command of test converter; i_{dref} = 2 A, i_{qref} = 0 A.

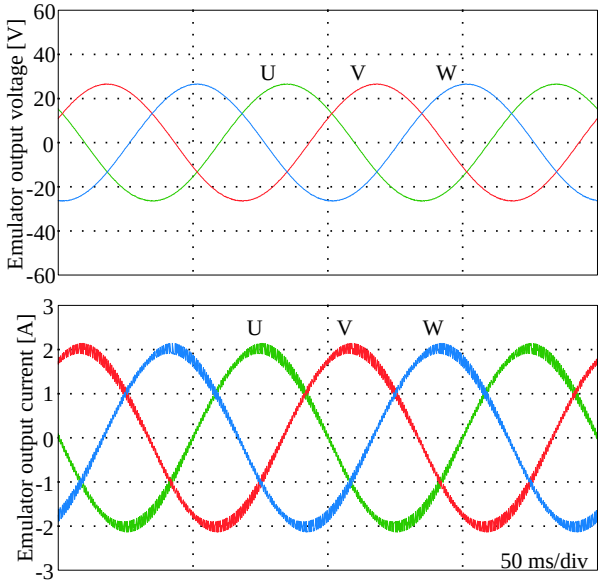

(a) Emulator output voltage and current.

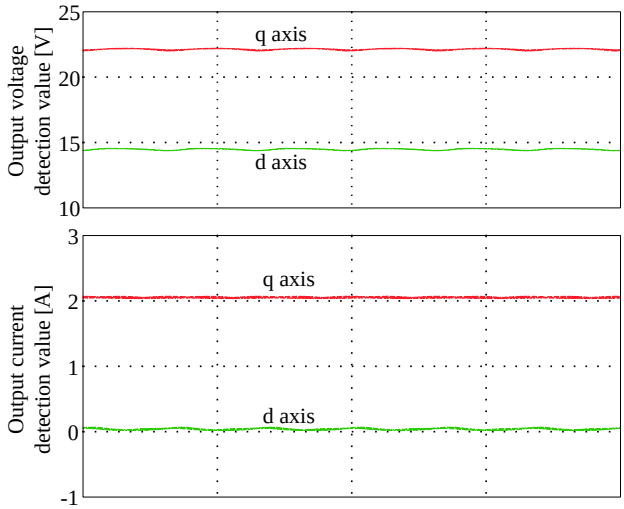

(b) Emulator output voltage and current detection value (dq axis).

Fig. 5. Simulation waveforms for wind turbine emulation. The current command of test converter; i_{dref} = 0 A, i_{qref} = -2 A.

II(a) are derived from the current command of the test converter. In Table II(a), error occurs between the theoretical and simulation value of the emulator output voltage. However, the error rate between the theoretical and simulation value is small as less than 5.0 %. Thus, the validity of the generator emulator operation is shown by the simulation results. In addition, the theoretical values of the emulator output voltage in Table II(b) are derived from the current detection value of the emulator. In Table II(b), the simulation output voltage is match to the theoretical value without error. Therefore, the factor of the error between the simulation and theoretical value of the emulator output voltage in Table II(a) occurs due to the error between the current command of the test converter and the output current of the emulator.

IV. Experimental Results

In this experiment, the experimental conditions shown in Table I are used for the emulation system. The current control response of the emulator is 40 times for the test converter. Moreover, the output frequency of the emulator is 10 Hz. In addition, the two LPF for the emulator output voltage detection are also applied to the experimental circuit. Note that the test converter current command direction is defined as that the positive direction is from the test converter to the emulator, the emulator current command direction is defined as that the positive direction is from the emulator to the test converter, respectively.

Figure 6 shows the operation waveforms of the emulator connected to the test converter which the d-axis current of -2 A

TABLE II. ERROR BETWEEN SIMULATION VALUE AND THEORETIACL VALUE IN SIMULATION RESULTS.

(a) Theoretical value: Derived from output current command of test converter.

		Measure [V]	Theory [V]	Error
Fig. 4	v_{ddet}	11.9	11.4	4.4%
	v_{qdet}	38.8	39.4	1.5%
Fig. 5	v_{ddet}	14.5	14.3	1.4%
	v_{qdet}	22.1	22.5	1.8%

(b) Theoretical value: Derived from output current detection value.

		Measure [V]	Theory [V]	Error
Fig. 4	v_{ddet}	11.9	11.9	0%
	v_{qdet}	38.8	38.8	0%
Fig. 5	v_{ddet}	14.5	14.5	0%
	v_{qdet}	22.1	22.1	0%

(c) Emulator current detection value and current command of test converter.

		Detection [A]	Command [A]
Fig. 4	i_d	1.97	2.0
	i_q	-0.08	0
Fig. 5	i_d	-0.04	0
	i_q	-2.05	-2.0

is injected from the emulator to the test converter. In Fig. 6 (a), the output current amplitude of the emulator follows to the current command of the test converter. In Fig. 6 (b), the current command detection value is match to the current command of dq axis. Thus, the emulator output current is follows to the current command of the test converter. Moreover, the output current distortion is low. Furthermore, the U phase output current in Fig. 6 is peak value when the phase is 0 degree. Thus, the current is output based on the phase information.

Figure 7 shows the operation waveforms of the emulator connected to the test converter which the q-axis current of 2 A is injected from the emulator to the test converter. The output current amplitude of the emulator in Fig. 7 also follows to the current command of the test converter. Moreover, the U phase output current in Fig. 7 is zero when the phase is 0 degree. Thus, the current is output based on the phase information.

Table III shows the comparison of the output voltage between the experimental results and theoretical values. The theoretical value of the output voltage is derived by the motor equation with the current command of the test converter. The error rates of the output voltage detection value v_{ddet}, v_{qdet} in Fig. 6 are 17.5% and 2.03%. The error rates of tfhe output voltage detection value v_{ddet}, v_{qdet} in Fig. 7 are 7.69% and 7.56%. Thus, the error rates of the output voltage detection value in dq axis are less than 17.5% in the experimental conditions. The cause of the error for 17.5% in Fig. 6 occur due to the voltage detection error, and the reduction of voltage detection

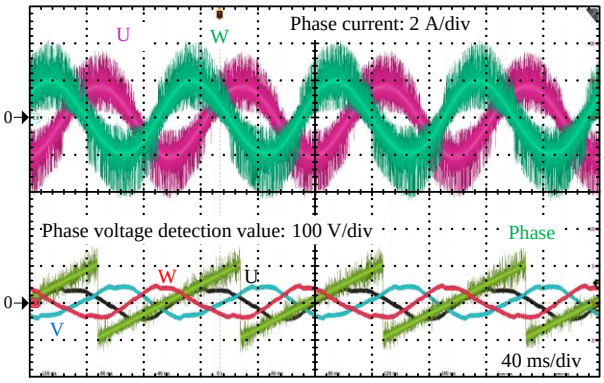

(a) Emulator phase voltage detection value with analog LPF, and emulator output current measured value.

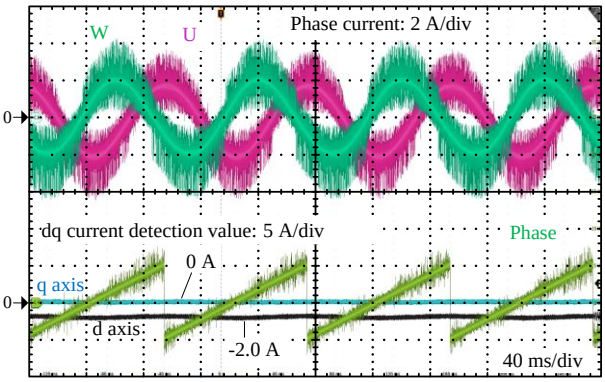

(b) Emulator output current detection value in dq axis, and emulator output current measured value.

Fig. 6. Experimental waveforms for wind turbine emulation. The command of test converter; i_{dref} = 2 A, i_{qref} = 0 A. Thus, the emulator output current follows the current command of the test converter.

resolution by operating at low voltage. Therefore, the output voltage for the output current is output based on the motor equations. Consequently, the validity of the emulator was confirmed in the experimental results. Hence, the emulator operated when the current control response of the emulator is separated from the current control response of the test converter.

V. CONCLUSION

This paper proposed the emulation system which simulates the wind turbine system. The output current and voltage of the emulator were output based on the current command of the test converter and the motor equations. The error rates of the output voltage detection values were less than 17.5% compared with the theoretical values.

Future work is to consider increasing the current control response for the test converter.

REFERENCES

[1] K. Motoyoshi, H. Kometani, N. Sora, and S. Maeda, “Large-Scale 3D Electromagnetic Field Analysis for Estimation of Stator End Region Loss in Turbine Generators,” *IEEJ Journal of Industry Applications*, vol. 6, no. 6, pp. 340-345, 2017.

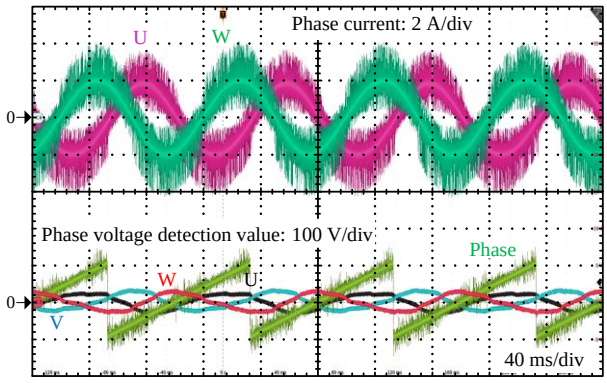

(a) Emulator phase voltage detection value with analog LPF, and emulator output current measured value.

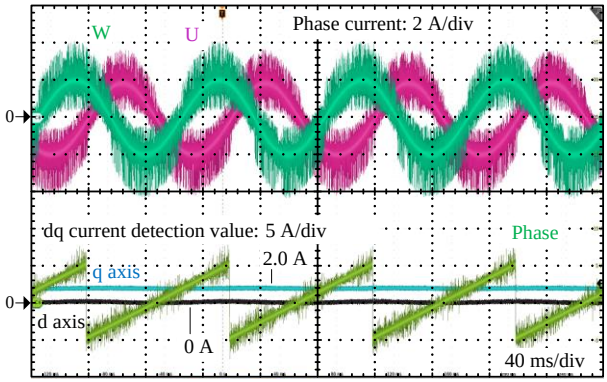

(b) Emulator output current detection value in dq axis, and emulator output current measured value.

Fig. 7. Experimental waveforms for wind turbine emulation. The command of test converter; i_{dref} = 0 A, i_{qref} = -2 A. Thus, the emulator output current follows the current command of the test converter.

TABLE III. ERROR BETWEEN MEASUREMENT VALUE AND THEORETICAL VALUE IN EXPERIMENTAL RESULTS.

		Measure [V]	Theory [V]	Error
Fig. 6	v_{ddet}	13.4	11.4	17.5%
	v_{qdet}	40.2	39.4	2.03%
Fig. 7	v_{ddet}	15.4	14.3	7.69%
	v_{qdet}	24.2	22.5	7.56%

[2] Z. Zhang, H. Fang, F. Gao, J. Rodríguez and R. Kennel, "Multiple-Vector Model Predictive Power Control for Grid-Tied Wind Turbine System With Enhanced Steady-State Control Performance," *IEEE Trans. Ind. Electron.*, vol. 64, no. 8, pp. 6287-6298, 2017.

[3] Z. Chen, J. M. Guerrero and F. Blaabjerg, "A Review of the State of the Art of Power Electronics for Wind Turbines," *IEEE Trans. Power Electron.*, vol. 24, no. 8, pp. 1859-1875, 2009.

[4] K. Ma, M. Liserre, F. Blaabjerg and T. Kerekes, "Thermal Loading and Lifetime Estimation for Power Device Considering Mission Profiles in Wind Power Converter," *IEEE Trans. Power Electron.*, vol. 30, no. 2, pp. 590-602, 2015.

[5] C. Haidar, R. Boutarfa, S. Harmand, "Fluid Flow and Convective Heat Transfer Analysis on a Rotor of Wind Turbine Alternator with an Impinging Jet," *International Journal of Renewable Energy Research*, Vol.9, No.3, pp. 1144-1153, 2019.

[6] J. Hussain, M. Hussain, S. Raza, M. Siddique, "Power Quality Improvement of Grid Connected Wind Energy System Using DSTATCOM-BESS," *International Journal of Renewable Energy Research*, Vol.9, No.3, pp. 1388-1397, 2019.

[7] V. Mishra, R. D. Shukla, P. Gupta, "An approach towards Application of Semiconductor Electronics Converter in Autonomous DFIM based Wind Energy Generation System: A Review," *International Journal of Smart Grid*, Vol.3, No.3, pp. 152-162, 2019.

[8] T. Messo, R. Luhtala, A. Aapro, and T. Roinila, "Accurate Impedance Model of a Grid-Connected Inverter for Small-Signal Stability Assessment in High-Impedance Grids," *IEEJ Journal of Industry Applications*, vol. 8, no. 3, pp. 488-496, 2019.

[9] A. Abokhalil "Grid Connection Control of DFIG for Variable Speed Wind Turbines under Turbulent Conditions," *International Journal of Renewable Energy Research*, Vol.9, No.3, pp. 1260-1271, 2019.

[10] H. Benbouhenni, "Application of Five-Level NPC Inverter in DPC-ANN of Doubly Fed Induction Generator for Wind Power Generation Systems," *International Journal of Smart Grid*, Vol.3, No.3, pp. 128-137, 2019.

[11] H. Benbouhenni, "Application of seven-level neural space vector PWM in direct vector control system of doubly fed induction generator for wind turbine," *International Journal of Smart Grid*, Vol.3, No.3, pp. 163-171, 2019.

[12] Akihiro Ura, Masayuki Sanada, Shigeo Morimoto, and Yukinori Inoue, "Influence of Structural Differences on Motor Characteristics of Concentrated Winding IPMSMs Obtained by Automatic Design," *IEEJ Journal of Industry Applications*, vol. 8, no. 3, pp. 458-464, 2019.

[13] Yuki Shimizu, Shigeo Morimoto, Masayuki Sanada, and Yukinori Inoue, "Influence of Permanent Magnet Properties and Arrangement on Performance of IPMSMs for Automotive Applications," *IEEJ Journal of Industry Applications*, vol. 6, no. 6, pp. 401-408, 2017.

[14] K. Saito and H. Akagi, "A Real-Time Real-Power Emulator of a Medium-Voltage High-Speed Induction Motor Coupled with a Mechanical Load," *in Proc. 2018 IEEE Energy Conversion Congress and Expo.* (*ECCE*), pp. 5242-5249, 2018.

[15] A. Castro, P. Zuniga, F. A. Uribe and E. Barocio, "Synchronous Generator Emulator Prototype as a Testbed for Electric Equipment," *IEEE Trans. Energy Conversion*, vol. 30, no. 1, pp. 404-406, 2015.

[16] J. Wang, L. Yang, Y. Ma, J. Wang, L. M. Tolbert, F. Wang, K. Tomsovic, "Static and Dynamic Power System Load Emulation in a Converter-Based Reconfigurable Power Grid Emulator," *IEEE Trans. Power Electron.*, vol. 31, no. 4, pp. 3239-3251, 2016.

[17] K. Luo, W. Shi, Y. Chi, Q. Wu and W. Wang, "Stability and accuracy considerations in the design and implementation of wind turbine power hardware in the loop platform," *in CSEE Journal of Power and Energy Systems*, vol. 3, no. 2, pp. 167-175, 2017.

[18] W. Ren, M. Steurer and T. L. Baldwin, "An Effective Method for Evaluating the Accuracy of Power Hardware-in-the-Loop Simulations," *IEEE Trans. Ind. Appl.*, vol. 45, no. 4, pp. 1484-1490, 2009.

[19] W. Ren, M. Steurer, and T. L. Baldwin, "Improve the stability and the accuracy of power hardware-in-the-loop simulation by selecting appropriate interface algorithms," *IEEE Trans. Ind. Appl.*, vol. 44, no. 4, pp. 1286-1294, 2008.

[20] A.Viehweider,G. Lauss, and L. Felix, "Stabilization of power hardware-inthe-loop simulations of electric energy systems," Simul. Modelling Practice Theory, vol. 19, no. 7, pp. 1699-1708, 2011.

[21] P. Kundur, "Power System Stability and Control," New York, NY, USA: McGraw-Hill, 1994.

[22] R. Krishnan, "Electric Motor Drives: Modeling, Analysis, and Control," Englewood Cliffs, NJ, USA: Prentice-Hall, 2001.